Article

Cell Reports

Mechanical Stress Regulates Epithelial Tissue Integrity and Stiffness through the FGFR/Erk2 Signaling Pathway during Embryogenesis

Graphical Abstract

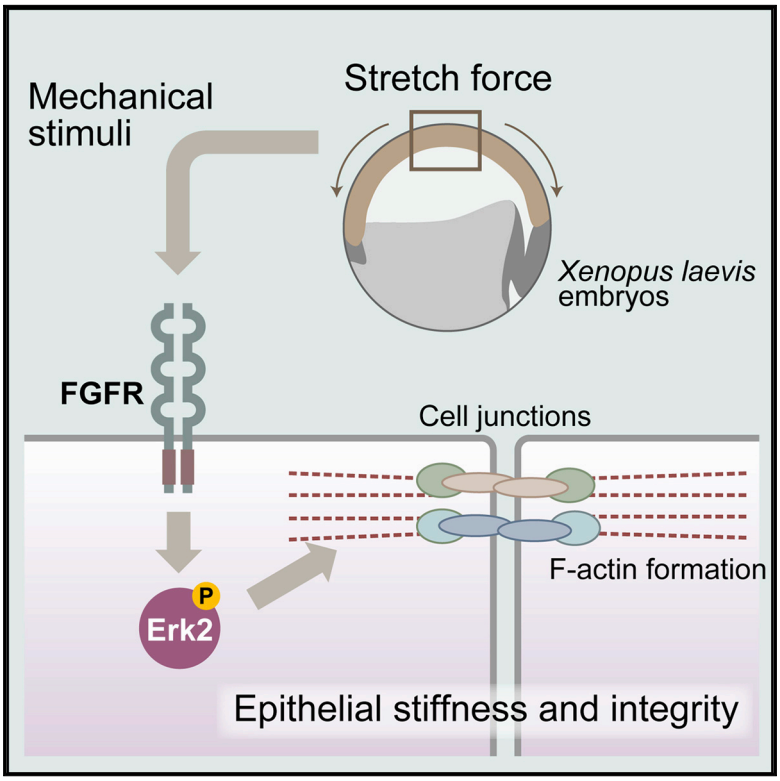

Highlights

- Stretching of the ectodermal tissue of the *Xenopus* embryo activates Erk2
- The stretch force phosphorylates Erk2 through FGFR in a ligand-independent manner
- Force-induced FGFR/Erk2 signaling enhances apical junctional structures
- This system increases epithelial stiffness and integrity during gastrulation

Authors

Noriyuki Kinoshita, Yutaka Hashimoto, Naoko Yasue, Makoto Suzuki, Ileana M. Cristea, Naoto Ueno

Correspondence

icristea@princeton.edu (I.M.C.), nueno@nibb.ac.jp (N.U.)

In Brief

Physical forces generated by morphogenetic movements are a critical component of embryogenesis. In this study, Kinoshita et al. demonstrate that stretching of the ectodermal tissue of the *Xenopus* embryo activates the FGF receptor/Erk2 pathway, which in turn enhances the apical junctional structure and increases epithelial stiffness and integrity during gastrulation.

Kinoshita et al., 2020, Cell Reports *30*, 3875–3888
March 17, 2020
https://doi.org/10.1016/j.celrep.2020.02.074

CellPress

Cell Reports
Article

Mechanical Stress Regulates Epithelial Tissue Integrity and Stiffness through the FGFR/Erk2 Signaling Pathway during Embryogenesis

Noriyuki Kinoshita,[1,2] Yutaka Hashimoto,[1,3,4,5] Naoko Yasue,[1] Makoto Suzuki,[1,2,6] Ileana M. Cristea,[4,*] and Naoto Ueno[1,2,7,*]

[1]Division of Morphogenesis, Department of Developmental Biology, National Institute for Basic Biology, National Institutes of Natural Sciences, Okazaki, Aichi 444-8585, Japan
[2]School of Life Science, SOKENDAI (The Graduate University for Advanced Studies), Okazaki, Aichi 444-8585, Japan
[3]International Research Collaboration Center, National Institutes of Natural Sciences, Tokyo 105-0001, Japan
[4]Department of Molecular Biology, Princeton University, Lewis Thomas Laboratory, Washington Road, Princeton, NJ 08544, USA
[5]Present address: Department of Cell Biology, Nagoya City University Graduate School of Medicine Sciences, Nagoya, Aichi 467-8601, Japan
[6]Present address: Amphibian Research Center, Hiroshima University, Higashi-Hiroshima, Hiroshima 739-8526, Japan
[7]Lead Contact
*Correspondence: icristea@princeton.edu (I.M.C.), nueno@nibb.ac.jp (N.U.)
https://doi.org/10.1016/j.celrep.2020.02.074

SUMMARY

Physical forces generated by tissue-tissue interactions are a critical component of embryogenesis, aiding the formation of organs in a coordinated manner. In this study, using *Xenopus laevis* embryos and phosphoproteome analyses, we uncover the rapid activation of the mitogen-activated protein (MAP) kinase Erk2 upon stimulation with centrifugal, compression, or stretching force. We demonstrate that Erk2 induces the remodeling of cytoskeletal proteins, including F-actin, an embryonic cadherin C-cadherin, and the tight junction protein ZO-1. We show these force-dependent changes to be prerequisites for the enhancement of cellular junctions and tissue stiffening during early embryogenesis. Furthermore, Erk2 activation is FGFR1 dependent while not requiring fibroblast growth factor (FGF) ligands, suggesting that cell/tissue deformation triggers receptor activation in the absence of ligands. These findings establish previously unrecognized functions for mechanical forces in embryogenesis and reveal its underlying force-induced signaling pathways.

INTRODUCTION

During the early development of animals, groups of differentiated cells vigorously move within the embryo in an orchestrated manner. Accordingly, tissue architectures are dramatically remodeled during organogenesis. *In vivo*, cells are attached to each other through cell-cell interaction structures, such as adherens and tight junction proteins, and to extracellular substrates through cell-substrate interaction molecules, such as integrin and fibronectin (Ramos et al., 1996; Winklbauer, 2012). Therefore, the status or morphogenesis of one population of cells influences the behavior of their neighboring cells. Such influences are thought to be initially mediated physically rather than chemically, as mechanical cues are transmitted at the interface of tissues. One example is the gastrulation cell movement. In the *Xenopus* embryo, convergent extension (CE) and convergent thickening of the mesoderm generate forces for involution and blastopore closure during gastrulation (Shook et al., 2018; Zhou et al., 2015). The leading-edge cells of involuted mesoderms actively migrate toward the future anterior side of the embryo and physically pull the following axial mesoderm cells, which are less migratory. This movement establishes the proper final topology of the three germ layer—namely, the ectoderm, mesoderm, and endoderm—to shape the embryo (Davidson et al., 2002). Pulling forces are also essential for normal CE movements in notochord morphogenesis (Hara et al., 2013). Furthermore, the physical interaction of the leading-edge cells with the following cells is required for the former cells to acquire the polarity information for anterior migration (Weber et al., 2012). A recent study revealed that the elongating notochord along the anterior-posterior axis in CE physically pushes the posterior domain of the axial mesoderm, which serves as a reservoir of progenitor cells of presomitic mesoderms (Xiong et al., 2018). In mouse embryogenesis, external mechanical forces exerted by the interaction between the embryo and the maternal uterine tissues are critical for establishing the anterior-posterior axis; they directly control the location of the distal visceral endoderm (DVE formation) at the distal tip (Hiramatsu et al., 2013). More recently, it has been shown that luminal pressure, which is an internal force during blastocyst development, increases cell cortical tension and tissue stiffness of the trophectoderm (Chan et al., 2019). All of these findings suggest that physical force may be a key driver for the morphogenesis of early embryos, although the mechanisms underlying these phenomena remain poorly understood.

To understand the contribution of physical forces to embryogenesis, it is essential to investigate how embryonic cells sense such forces and how mechanical signals are transmitted and interpreted by the cells. To address these questions, we previously

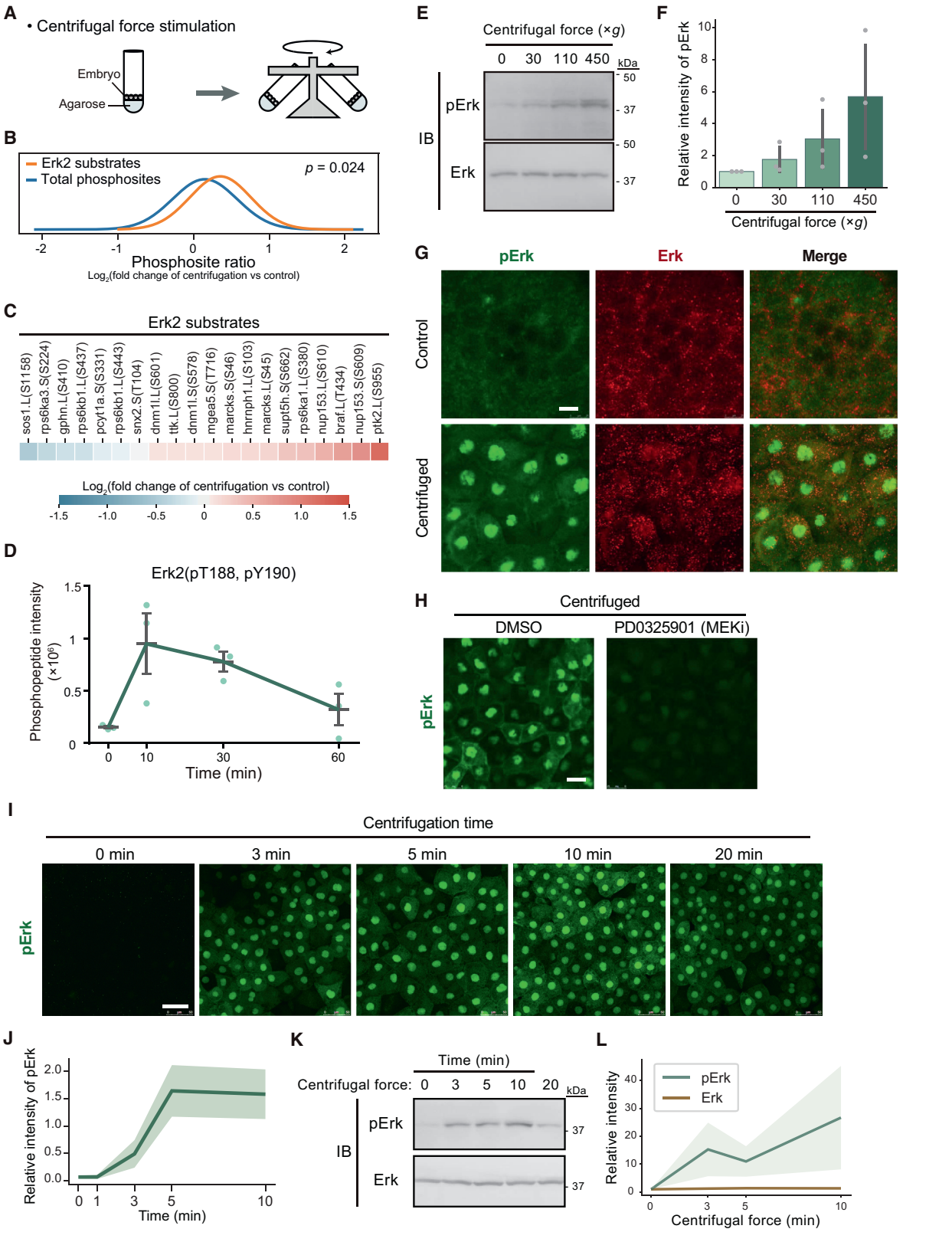

(legend on next page)

investigated the chemical response of embryos to physical force exerted by centrifugation. Centrifugal force initially compresses embryos, and as a consequence, it induces deformation of the embryo from a spherical to a flattened shape. This deformation leads to a drastic change in the phosphoproteomic profile (Hashimoto et al., 2019), despite the fact that the centrifuged embryo assumed its original morphology and developed without displaying evident abnormalities. In the present study, we identified a pathway by which the force application impacts the embryonic ectoderm, remodeling cell-cell junctions to increase tissue integrity. We also compared centrifugal force to other force applications, compression and stretching, and found that these different types of force application result in similar biochemical and cellular changes of the embryonic tissue.

A fundamental aspect of mechanoresponse is the ability of cells to sense mechanical stresses and consequently trigger cascades of chemical reactions. Given the known contribution of phosphorylation to rapid signaling events, alterations in protein phosphorylation may represent some of the earliest chemical changes in response to mechanical stresses. In our previous study, we used quantitative mass spectrometry to globally investigate force-induced phosphorylation changes in *Xenopus laevis* embryos subjected to centrifugation and discovered several functional classes of proteins that displayed rapid increases in phosphorylation upon centrifugation (Hashimoto et al., 2019). Here, we characterize Erk, a mitogen-activated protein kinase (MAPK) family kinase that is activated through receptor tyrosine kinases (RTKs), establishing it as an early target for mechanical stress-dependent phosphorylation. Erk translocated from the cytoplasm to the nucleus upon its phosphorylation. Furthermore, we found that tissue stiffness was increased by the centrifugal and other forces, most likely via the remodeling of actomyosin during early development.

Erk kinases are known to be activated in cells upon stimulation with various growth factors (Seger and Krebs, 1995). Among these factors, FGFs (fibroblast growth factors) and their receptor(s) play critical roles in cell differentiation and cell behaviors during development. However, against our expectation that FGF ligands would be involved in Erk activation, we found that a ligand-independent activation of FGF receptor(s) is involved in the mechanical-force-dependent Erk phosphorylation and its subsequent nuclear translocation.

Altogether, our findings indicate that in addition to the conventional ligand-dependent RTK pathways, previously unrecognized mechanoresponse pathways help to regulate cytoskeletal dynamics and maintain tissue integrity, including during development.

RESULTS

Erk2 Is a Target of Force-Dependent Phosphorylation

Although it is increasingly recognized that mechanical stimuli influence a variety of biological processes, it remains poorly understood how cells sense and respond to mechanical forces, especially in whole organisms such as developing embryos. In our previous work (Hashimoto et al., 2019), we established a method for the phosphoproteome analysis of *Xenopus laevis* embryos under the mechanical stress conditions (i.e., centrifugation and compression). We briefly treated the embryos with proteinase K to loosen the vitelline membrane so that embryos can easily be deformed in response to mechanical force. Importantly, the force-induced morphological changes were reversible, as most of the embryos underwent normal gastrulation (see Method Details).

Under our experimental conditions, we previously found that the mechanical force by centrifugation (Figure 1A) increased the phosphorylation levels of specific functional classes of proteins (Hashimoto et al., 2019). Among these, we focused on Erk2/MAPK1 substrates that had significantly elevated phosphorylated levels, suggesting that Erk2 is activated in response to force (Figures 1B and 1C). A time-course analysis showed that Erk2 phosphorylation (pErk) is induced rapidly, being phosphorylated after a 10-min centrifugation at a threonine (T188) and tyrosine (Y190), which is then followed by a gradual decrease in phosphorylation (Figure 1D). We confirmed these findings by western blotting with antibodies against phosphorylated Erk2 (anti-pErk2), demonstrating that Erk2 phosphorylation was increased by centrifugation in a force-dependent manner (Figures 1E and 1F). We showed that Erk2 phosphorylation occurred in response to a force load as small as 30 × *g*. These results indicate that Erk2 is a sensitive target of the mechanical force applied to *Xenopus* embryos.

To understand the dynamics of the pErk2 protein response to mechanical force, we next used immunofluorescence

Figure 1. Mechanical Stress by Centrifugation Activates Erk2

(A) Schematic diagram of the force applied to embryos by centrifugation.

(B) Normal density curves of the ratio of phosphosites between centrifuged and control conditions from phosphoproteomic data. Blue and orange lines represent the density curve in the total phosphosites and that in Erk2 substrates, respectively. The p value represents statistical significance evaluated by the Mann-Whitney U test.

(C) Heatmap of the Erk2 substrates (phosphosites) used in (B).

(D) Phosphopeptides of Erk2 were quantified by phosphoproteomic analysis during the indicated times. Data are means ± SEM from three biological replicates.

(E) Western blot using anti-pErk1/2 and anti-Erk1/2 antibodies.

(F) The quantification of the pErk intensities examined as in (E). Three independent experiments were quantified. Error bar: standard deviation (SD).

(G) Immunofluorescence using anti-pErk and anti-total Erk1/2 antibodies. Cells in the animal hemisphere were observed. Scale bar: 25 μm.

(H) Embryos were treated with DMSO or the Mek inhibitor PD0325901 (25 μM). Scale bar: 25 μm.

(I) Time course of Erk2 phosphorylation.

(J) The quantification of the pErk intensities in the nuclei examined as in (I). Scale bar: 50 μm.

(K) Western blot using anti-pErk1/2 and anti-Erk1/2 antibodies.

(L) The quantification of the intensities of pErk and Erk examined as in (K). Data are mean from two independent experiments. Error bar: SD.

See also Figure S1.

microscopy to examine the change over time in the intracellular localization of total Erk2 and pErk2 in *Xenopus* embryos. We specifically monitored the outer surface (ectoderm) cells in the animal hemisphere of intact embryos at stage (st.) 10.5. As shown in Figure 1G, in the control embryo, the total Erk2 was localized mainly to cytoplasmic puncta, and the pErk2 level was very low. After centrifugation, pErk2 became evident in the nucleus and at the plasma membrane, whereas most of the total Erk2 remained in the cytoplasmic puncta. Treating the cells with the Mek inhibitor PD0325901 markedly suppressed the pErk2 signals (Figure 1H), indicating that the centrifugation-induced anti-pErk2 signals in the nucleus and plasma membrane depended on the Mek activity.

We next examined the time course of Erk2 activation. Embryos were centrifuged at 450 × *g* for different lengths of time, and then Erk2 activation was assessed by immunofluorescence microscopy. The pErk2 was detectable within a 3-min centrifugation and peaked after 10 min (Figures 1I–1L). The nuclear localization of pErk2 is likely attributed to Erk2 being fully activated upon its phosphorylation (Chen et al., 1992). The accumulated pErk2 signal by centrifugation (450 × *g* for 10 min) was rapidly decreased within 15 to 20 min (Figures S1A–S1D).

Next, we tested whether the Erk2 activation required *de novo* protein synthesis. As shown in Figures S1E and S1F, neither of the protein synthesis inhibitors cycloheximide and anisomycin affected the Erk2 activation at concentrations sufficient to block the onset of gastrulation, suggesting that *de novo* protein synthesis was not required for the Erk2 activation induced by centrifugation. These results indicated that the activation of Erk2 by mechanical stress likely represents a rapid cellular response that does not require transcription or translation.

Tissue Deformation Induces Erk2 Phosphorylation

Centrifugation of whole embryos induces a flattening of the embryonic shape, causing abnormal contacts between the ectoderm and other tissues, such as the mesoderm and endoderm, which secrete signaling molecules (e.g., embryonic FGF [FGF4]) (Isaacs et al., 1992). Therefore, to exclude the possibility that such signaling molecules may induce Erk2 activation, we excised a part of the ectoderm (animal cap explant) and subjected it to centrifugation. Animal cap explants were isolated at st. 9, cultured until sibling embryos reached st. 10.5, and then centrifuged. Even in this condition, the centrifuged explants were flattened, and Erk2 became phosphorylated similarly to intact embryos (Figure S1G), indicating that the mesoderm or endoderm are dispensable and that the ectodermal tissue is sufficient for this mechanoresponse.

As the mechanism of Erk2 activation, we postulated two possibilities. One possibility is via embryonic deformation, and the other is via displacement of the nucleus or other organelles induced by the direct gravitational force to the cells. In order to test these possibilities, we used embryos with intact vitelline membranes, instead of embryos treated with proteinase K, as described above. The embryos with intact vitelline membrane underwent little deformation, and the Erk2 activation was significantly attenuated (Figures S1H and S1I). This observation indicates that tissue deformation, rather than gravitational force, is the likely cause of the Erk2 activation.

In addition to centrifugation, we applied a different type of force—compression—to the embryos (Figure 2A) by using a coverslip placed on top of st. 10.5 embryos for 5 min. The embryos were deformed to approximately 50% and 30% of their original heights, which was associated with a flattening and surface area expansion of the embryos by 1.5- and 2.0-fold, respectively. Similar to centrifugation, compression also induced Erk2 phosphorylation (Figures 2B and 2C), supporting our hypothesis that tissue deformation induces Erk2 activation.

Furthermore, we also tested the application of stretching stimulation to the embryonic tissue. Animal cap explants excised at st. 9.5 (before gastrulation) were placed on a fibronectin-coated silicone chamber and left to adhere to the substrate (Figure 2D, left). When sibling embryos reached st. 10.5, the explants were mechanically stretched by pulling the chamber until they elongated to 1.5-fold and then kept in this state for 5 min before relaxation (Figure 2D, right). Erk2 phosphorylation was markedly induced in response to stretching. Altogether, we conclude that activation of the Erk signaling pathway is a common response to mechanical forces that cause cell/tissue deformation.

Erk2 Phosphorylation Induces the Remodeling of Cell Junctions and Increases Tissue Stiffness

To investigate whether the mechanical force and Erk2 activation affected the overall cytoskeletal organization, we examined cross-sections of early gastrula embryos (st. 10.5) stained with fluorescent phalloidin to visualize F-actin (Figure 3A), focusing on the superficial layer of the animal hemisphere. In control embryos, F-actin was concentrated in the basolateral region. In contrast, in centrifuged embryos, more F-actin was accumulated in the apical region, indicating that mechanical force induced F-actin remodeling. In addition, the Mek inhibitor PD0325901 suppressed this apical accumulation, confirming that this F-actin remodeling was regulated by Erk2 (Figures 3A and 3B). We also found that C-cadherin, which was predominantly expressed in early *Xenopus* embryos, accumulated heavily at the cell junctions along with F-actin (Figure 3C). ZO-1, an important component of tight junctions, was also accumulated at tight junctions upon centrifugation, as we noted in the previous study (Figure 3C; also see Hashimoto et al. [2019]). We also confirmed the accumulation of C-cadherin and ZO-1 at the cell junctions in the compressed embryos (Figures S2A–S2C) and the accumulation of ZO-1 in the stretched animal cap explants (Figures S2D and S2E).

We speculated that the apical accumulation of F-actin and the junctional enhancement would affect the tissue stiffness of the embryonic surface. To test this possibility, we measured the stiffness of the embryos by atomic force microscopy (AFM) (Figure 3D). The stiffness of three or four points of the animal pole region in each embryo was measured, and Young's modulus at each point was calculated. This analysis showed that the average stiffness of the centrifuged embryos was twice that of the control embryos (Figure 3E). In addition, we found that this increase in stiffness was inhibited by PD0325901, indicating that the mechanical stress increased tissue stiffness through Erk2 activity.

We further confirmed our finding that Erk2 inhibition decreased tissue stiffness using another method (Figures 3F and 3G). In this experiment, the embryos were treated with

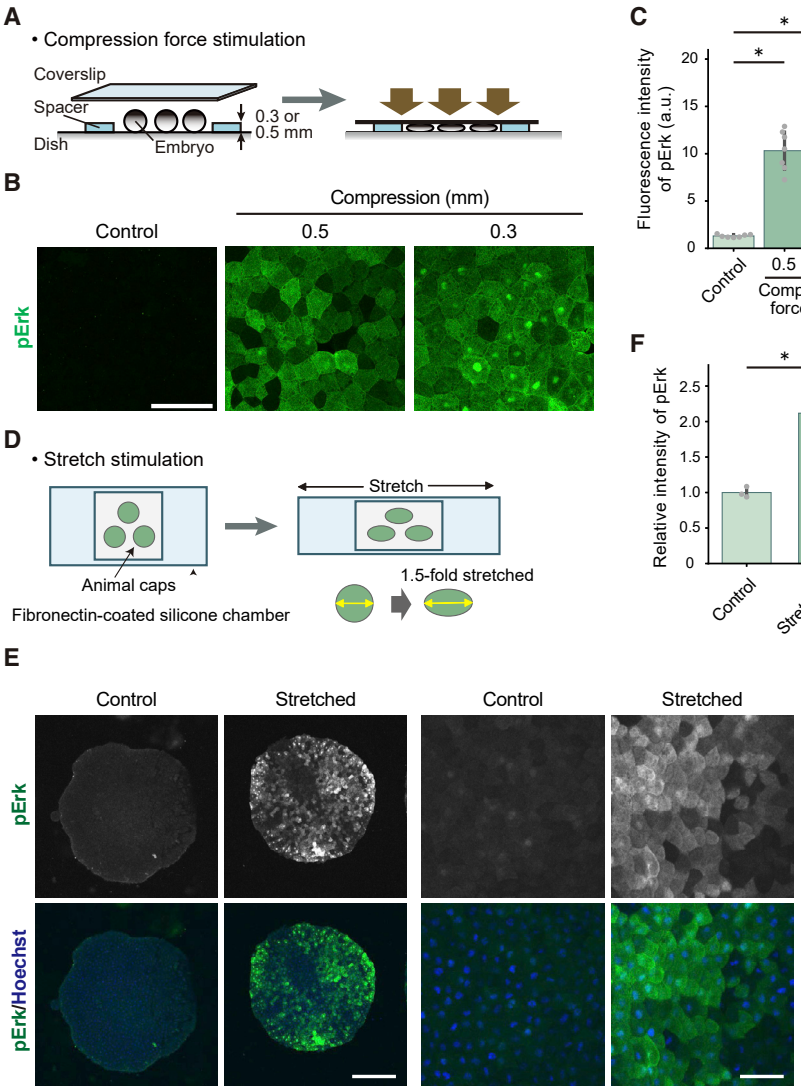

Figure 2. Mechanical Stress by Compression or Stretching Activates Erk2

(A) Schematic diagram of the force applied to embryos by compression.

(B) Immunofluorescence using anti-pErk antibodies. Cells in the animal hemisphere were observed. Scale bar: 100 μm.

(C) Fluorescent intensity of cells that were compressed for 5 min were quantified. n = 40 ~50 cells from three independent embryos for each condition. *p < 0.01.

(D) Schematic diagram of the force applied to embryos by stretching. The stretched chamber was kept for 5 min, and then the animal caps were fixed for immunofluorescence.

(E) Immunofluorescence using anti-pErk antibodies. Left panels: images of whole animal caps. Scale bar: 100 μm. Right panels: images at the cellular level from the apical side. Scale bar: 50 μm.

(F) Fluorescent intensity of three animal cap explants for each condition was quantified. *p < 0.01.

DMSO or PD0325901 and incubated in the culture medium 30 min prior to centrifugation. After centrifugation, the deformation of the embryos was quantified as the embryonic area when viewed from above. As shown in Figure 3G, the area of each embryo was increased as the centrifugation time increased. In the presence of PD0325901, the areas of the embryos were larger than those of controls, suggesting that the Mek/Erk2 pathway normally confers embryonic rigidity. Taken together, these results demonstrated that *Xenopus* embryos altered their actin cytoskeletal network and cell junctions to increase their surface stiffness in response to the mechanical force, and these reactions were regulated by the Erk2 signaling pathway.

FGF Receptor Plays an Essential Role in Mechanical-Force-Induced Erk2 Activation

To investigate how Erk2 is activated by mechanical force, we treated embryos with several kinase inhibitors and tested whether these treatments affected the mechanical-force-induced Erk2 activation. Among the tested inhibitors, we found that a broad-spectrum tyrosine kinase inhibitor, AG18 (Levitzki and Gazit, 1995), effectively reduced the Erk2 activation (Figure 4A). This finding suggested that protein tyrosine kinases (PTKs) might be involved in the Erk2 activation. It is well known that PTKs activate the Ras/Raf/Mek/Erk2 signaling pathway through Grb2/Sos (Clark et al., 1992). We therefore constructed a dominant-negative Grb2, which only contained the SH2 domain (Grb2-SH2), and expressed it in *Xenopus* embryos with membrane-tethered GFP (mGFP) as a lineage tracer in a mosaic manner. This construct was previously shown to block endogenous Grb2 and to compromise Erk2 activities (Gupta and Mayer, 1998). The treated embryos were centrifuged at the early gastrula stage (st. 10.5), followed by immunofluorescence microscopy with anti-pErk1/2 antibodies. As shown in Figure 4B, the Grb2-SH2-expressing cells had much lower nuclear Erk2 phosphorylation than did the control cells. These results indicated that upstream PTKs may activate the Mek/Erk pathway.

One of the well-characterized PTKs expressed during *Xenopus* embryogenesis is FGF receptor 1 (FGFR1). We therefore treated embryos with specific FGFR inhibitors, BGJ398 and SU5402 (Guagnano et al., 2011; Mohammadi et al., 1997), and found that they also suppressed the centrifugation-induced Erk2 activation (Figures 4C and 4D). Furthermore, we sought to inhibit FGFR1 tyrosine kinase by expressing two different dominant-negative FGFR1 mutants. One (FGFRΔC) has the extracellular domain and the transmembrane domain but lacks the entire cytoplasmic tyrosine kinase domain (Amaya et al., 1991). The other (FGFR-KRYF) has point mutations in Lys residues that are important for ATP

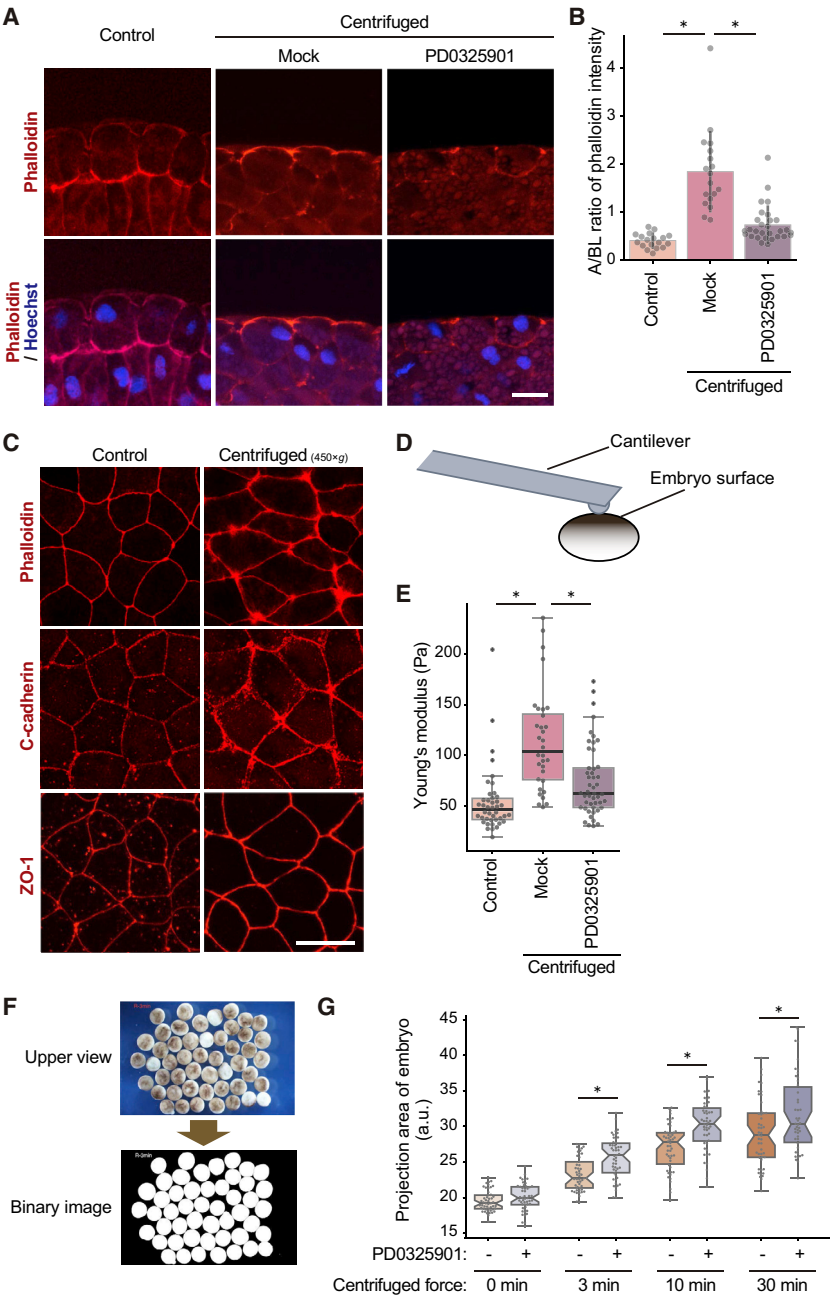

Figure 3. Erk2 Phosphorylation Induces Remodeling of Cell Junctions and Increases Tissue Stiffness

(A) Cross-section of embryos treated with DMSO or the Mek inhibitor PD0325901 (25 μM, 30 min prior to and during centrifugation at 450 × *g*, 10 min) and stained with fluorescent phalloidin and Hoechst 33342. Cells in the animal hemisphere were observed. Scale bar: 50 μm.

(B) Intensities of phalloidin fluorescence in the apical and basal sides of superficial layer cells were quantified. The y axis shows the ratio of apical to basal F-actin intensity. n = 18, 18, and 27, respectively. *p < 0.01.

(C) Embryos centrifuged at 450 × *g* for 10 min, and control embryos were stained with fluorescent phalloidin and with anti-C-cadherin and anti-ZO-1 antibodies. Scale bar: 50 μm.

(D) Embryonic stiffness was measured as Young's modulus by an atomic force microscope (AFM).

(E) The quantification of the embryonic stiffness examined as in (D). In total, 10∼15 embryos were prepared for each condition, and three to four points in the animal pole region of each embryo were measured.

(F). Schematic diagram to quantify the embryonic deformation. Deformation of the embryos was measured as the area of the binary image of the embryo from the upper view.

(G) Embryos were treated with DMSO or PD0325901 and centrifuged for the indicated time at 110 × *g*. The quantification of the embryonic deformation was examined as in (F). Graph shows the relative size of embryos with or without Mek inhibitor PD0325901. n = 46 ∼50 embryos. *p < 0.01.

See also Figure S2.

binding and in two Tyr residues essential for its autophosphorylation activity (Figure S3B) (Barone and Courtneidge, 1995; Furge et al., 2001). FGFRΔC inhibits the ligand-dependent tyrosine kinase activation (Amaya et al., 1991), and FGFR-KRYF is expected to inhibit the kinase itself regardless of its ligands. We expressed these mutants, respectively, with mGFP in *Xenopus* embryos, which were then centrifuged at the early gastrula stage. Interestingly, as shown in Figures 4E–4G, the FGFR-KRYF mutant blocked Erk2 activation, whereas FGFRΔC did not. As a proof of concept, we confirmed that both mutants are capable of inhibiting the endogenous Erk2 activation in the mesoderm, which is thought to occur in a ligand-dependent manner (Figure S3A). Taken together, the inability of FGFRΔC to inhibit centrifugation-induced FGFR signaling implied that centrifugation may activate the FGFR via an FGF-ligand-independent mechanism.

To gain further insights into the FGFR1-dependent signaling mechanism leading to Erk2 activation, we used two additional FGFR1 mutants, ΔC110 and ΔIgΔC110 (Figure S3B). The cytoplasmic domain of ΔC is only a few amino acids (aa) long, whereas that of ΔC110 is 110 aa longer. ΔIgΔC110 lacks most of the immunoglobulin domain, including the FGF-ligand-binding domain (Farrell and Breeze, 2018; Plotnikov et al., 1999). Interestingly, both of these mutants efficiently inhibited centrifugation-induced Erk2 phosphorylation (Figures S3C and S3D). Therefore, the cytoplasmic 110-aa region may play an important role in this mechanoresponse. The finding that ΔIgΔC110, which lacks the FGF-ligand-binding domain, can inhibit Erk2 activation strongly suggests that mechanical forces activate the Erk pathway through an alternative mechanism than the conventional FGF ligand-receptor interaction.

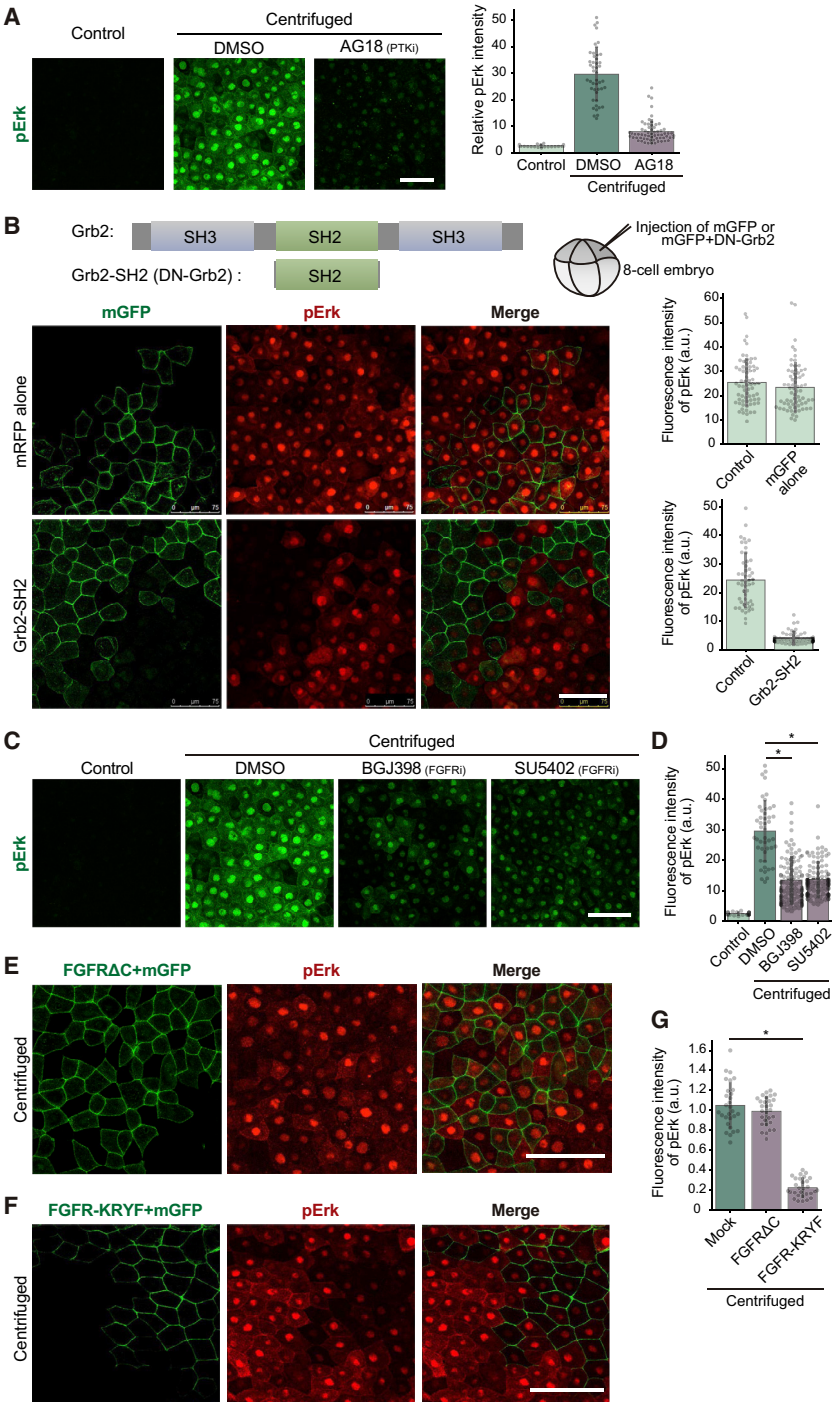

Figure 4. Erk2 Phosphorylation Induced by Centrifugation Requires FGFR Activity

(A) The broad-spectrum protein tyrosine kinase inhibitor (PTKi) AG18 (100 μM) inhibited the Erk2 activation. Scale bar: 50 μm.

(B) Dominant-negative (DN) Grb2 (Grb2-SH2) was expressed with mGFP as a lineage tracer in *Xenopus* embryos. The embryos were centrifuged and subjected to immunofluorescence analysis. The pERK intensity in cells with or without Grb2-SH2 expression was quantified. Scale bar: 75 μm.

(C) FGFR inhibitors BGJ398 (50 μM) and SU5402 (50 μM) reduced the Erk2 activation. The experiments were conducted at the same time with those of Figure 4A. Scale bar: 100 μm.

(D) Statistical data of (C). "Control" and "DMSO" are also identical to those of Figure 4A. *$p < 0.01$.

(E) Dominant-negative FGFR mutant (FGFRΔC) was expressed with mGFP, and embryos were centrifuged. Scale bar: 100 μm.

(F) Dominant-negative FGFR mutant (FGFR-KRYF) was expressed with mGFP, and embryos were centrifuged. Scale bar: 100 μm.

(G) Statistical data of (E) and (F). *$p < 0.01$.

See also Figure S3.

Mechanical Force Induces an Increase in FGFR Phosphorylation

To demonstrate that FGFR is indeed activated by centrifugation or compression, autophosphorylation of FGFR was monitored as an indicator for FGFR activation. In human FGFR1, Tyr635/654 are phosphorylated, and these residues are important for its activity (Mohammadi et al., 1996). In *Xenopus laevis* FGFR1, the corresponding residues are conserved, as are the surrounding residues, with over 100 aa in the sequence being identical to the human FGFR1 sequence. We thus used a commercially available anti-phospho-FGFR (Tyr635/654) antibody (anti-pFGFR) to examine whether FGFR phosphorylation increased in response to mechanical force. As shown in Figure 5A, centrifuged cells showed anti-pFGFR staining at the plasma membrane, whereas uncentrifuged control cells did not. In addition, the staining at the plasma membrane disappeared in FGFR-inhibitor-treated cells but was not affected in cells treated with the Mek inhibitor. A similar change was observed with dnFGFR- KRYF but not with dnFGFRΔC in the compressed embryo (Figure 5B). Accordingly, pErk2 phosphorylation induced by compression was significantly reduced in dnFGFR-KRYF-expressing cells (Figures S4A and S4B), consistent with our hypothesis that Erk2 is a downstream target for FGFR in the force-dependent pathway. These results indicate that FGFR is phosphorylated and activated in response to mechanical forces.

We have shown that mechanical forces induce the relocalization of F-actin, ZO-1, and C-cadherin (Figure 3C). In order to test whether these responses require the activation of the FGFR-Erk2 pathway, we again used Mek inhibitor PD0325901 and FGFR inhibitor BGJ398. Both inhibitors abolished the centrifugation-induced accumulation of C-cadherin and ZO-1 to the cell junction (Figures S4C and S4D).

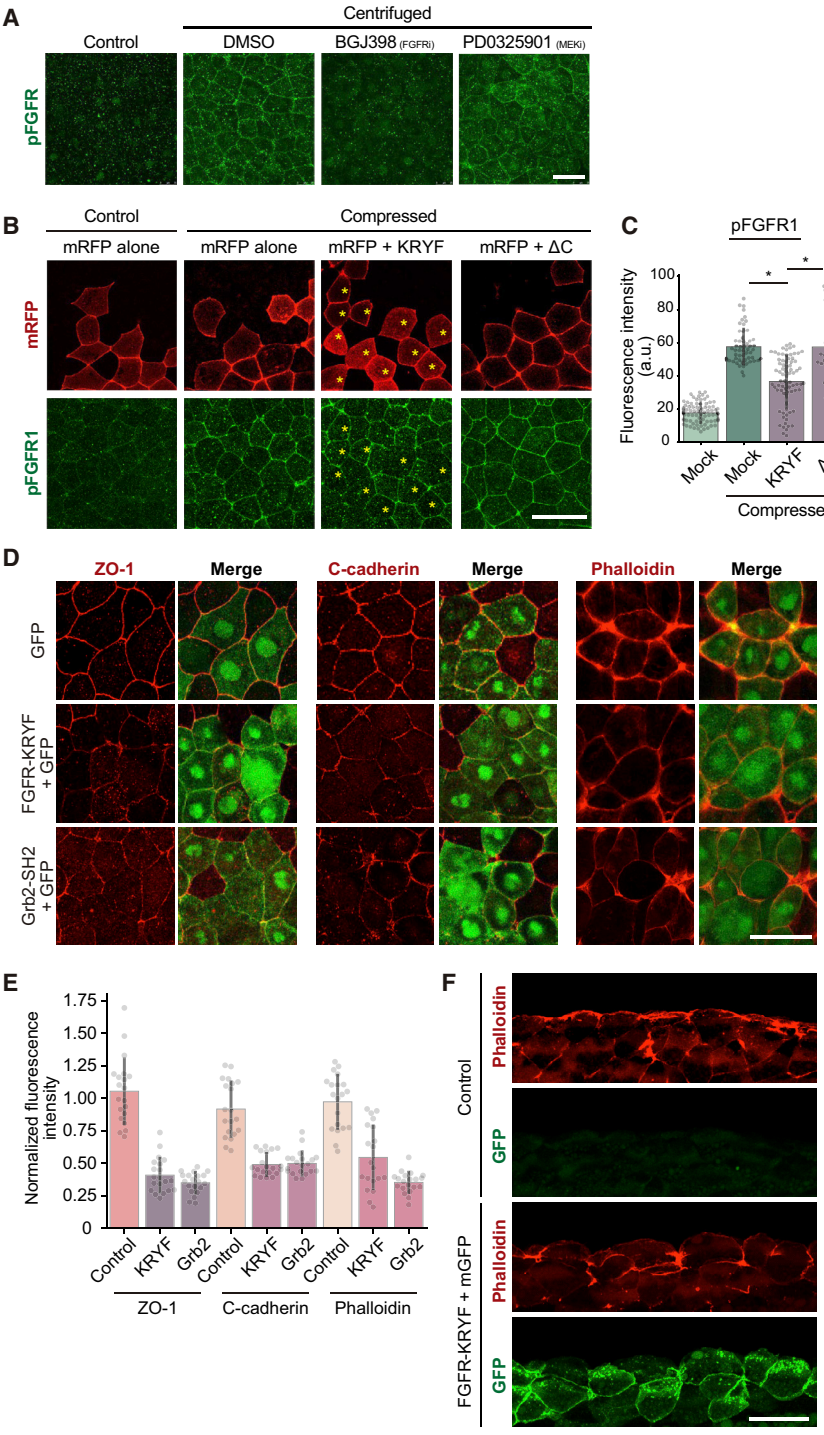

Figure 5. FGFR Is Phosphorylated in Response to Mechanical Stress

(A) Centrifuged embryos (450 × *g*, 10 min) were immunostained with anti-phosphorylated FGFR1 (pFGFR) antibodies. Centrifugation increased the staining on the plasma membrane. The FGFR inhibitor BGJ398 (50 μM) suppressed it, whereas the MEK inhibitor PD0325901 (25 μM) did not. Scale bar: 50 μm.

(B) mRFP mRNA with or without FGFR1 mutant mRNAs, FGFR-KRYF and ΔC, were injected into embryos at the four-cell stage. The embryos were compressed (0.3 mm, 5 min) at the early gastrula stage and immunostained with anti-pFGFR1 antibodies. The asterisks indicate KRYF-expressing cells. *$p < 0.01$. Scale bar: 50 μm.

(C) Statistical data of (B). *$p < 0.01$.

(D) mRNAs encoding FGFR-KRYF or Grb2-SH2 were co-injected with GFP mRNA at the four-cell stage. Embryos were centrifuged at 450 × *g* for 10 min and stained with indicated antibodies or phalloidin. Scale bar: 50 μm.

(E) Fluorescent intensity of the plasma membrane was quantified (n = 40).

(F) mRNAs encoding FGFR-KRYF were injected into four-cell embryos. At st. 10.5, embryos were centrifuged. After staining with fluorescent phalloidin, embryos were embedded in agarose gel and sectioned with vibratome. Upper panels: cells not expressing mGFP (control); lower panels: cells expressing KRYF and mGFP. Scale bar: 50 μm.

See also Figure S4.

The dominant-negative mutants FGFR-KRYF and Grb2-SH2 also blocked the accumulation of ZO-1, C-cadherin, and F-actin (Figures 5D and 5E). We further demonstrated by sectional view of the centrifuged embryos that the apical accumulation of F-actin induced by centrifugation was remarkably blocked by FGFR-KRYF (Figure 5F). These results revealed that the FGFR-Erk2 pathway is required for the F-actin reorganization and the junctional enhancement in response to the mechanical force.

FGFR-Erk2 Activation and Junction Remodeling during Normal Gastrulation

To explore the physiological significance of our findings, we examined the phosphorylation of FGFR and Erk2 in the ectoderm of a normal embryo during gastrulation. We focused on ectodermal cells undergoing epiboly movement, in which the ectodermal cell sheet in the animal hemisphere expands radially but with a preference toward posterior, eventually covering the whole embryo. We found that FGFR and Erk2 were phosphorylated in the st. 12 (late gastrula) embryos much more evidently than in the st. 10 embryos (Figures 6A and 6B). In contrast, neither FGFR nor Erk2 was phosphorylated in the animal caps cultured until st. 12, which did not undergo epiboly movement and were probably free from the tensile force generated by gastrulation movements. The phosphorylation of FGFR in the ectoderm was inhibited by FGFR-KRYF but not by ΔC (Figure 6C), suggesting that the FGFR-Erk2 pathway in the ectoderm may also be employed via a ligand-independent mechanism,

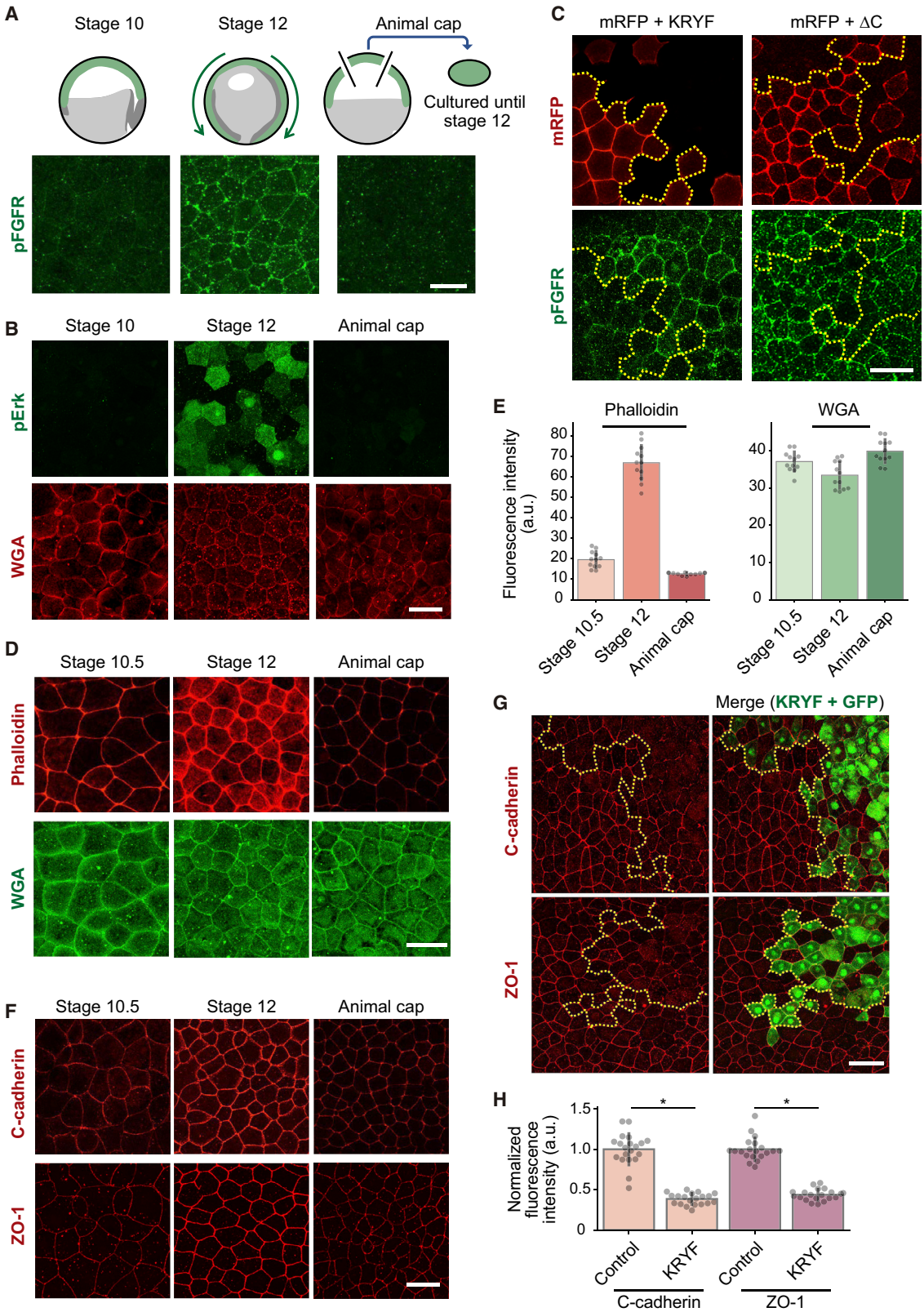

(legend on next page)

similar to the mechanoresponses upon centrifugation or compression. Furthermore, we found that F-actin, C-cadherin, and ZO-1 were significantly accumulated at the cell junction during gastrulation compared to those in animal caps (Figures 6D–6F). These changes were similar to the cellular response to the artificial mechanical stresses, such as centrifugation and compression. In the animal cap cells, the accumulation of these proteins was not observed consistently, suggesting that the FGFR-Erk2 pathway was not activated in the animal caps (Figures 6A and 6B). When FGFR-KRYF was expressed, the accumulation of C-cadherin and ZO-1 in st. 12 embryos was clearly abrogated (Figures 6G and 6H), indicating the necessity of FGFR signaling for this process. In addition, we observed that Erk2 inhibition by Mek inhibitor PD0325901 treatment immediately blocks gastrulation movements, including epiboly (Figure S4E), suggesting the importance of the role of the FGFR/Erk2 signaling in this process.

The activation of the FGFR/Erk2 pathway and junctional remodeling in the ectodermal cells during gastrulation suggests that these cells may be under tensile force generated by gastrulation movements. In the zebrafish embryos, the ectoderm area is thought to be under the stress of the stretching cell sheet due to the epiboly movement during gastrulation (Campinho et al., 2013; Hernández-Vega et al., 2017). Thus, we examined whether the cortical tension of ectoderm cells increases during *Xenopus* gastrulation by laser ablation (Figure 7A). mRNA-encoding mGFP was injected into the animal pole region. mGFP-expressing cells, which localized around the animal pole of the st. 10 embryos and in the anterior region of the st. 12 embryos, were subjected to laser ablation. As shown in Figures 7A–7C, the displacement rate after the ablation was much higher in st. 12 embryos than in st. 10 embryos. This indicates that the tensile stress to the ectodermal cells increases as the epiboly movement proceeds, and this tensile force may induce the FGFR-Erk2 activation and junctional remodeling.

As the tensile force increased and cell junctional structures seem to become more intense during gastrulation, we assumed that these changes might also contribute to the increase in embryonic stiffness. We measured the stiffness of the animal region of st. 10 embryos and the anterior region of st. 12 embryos by AFM. As shown in Figure 7D, st. 12 embryos were stiffer than st. 10 embryos. Stiffness of the animal caps isolated from st. 9.5 embryos and cultured until st. 12 was not increased as expected. Furthermore, the increased stiffness during gastrulation was inhibited by the expression of the FGFR-KRYF mutant (Figure 7E). Importantly, KRYF did not seem to affect the stiffness at st. 10.5. This suggests that FGFR signaling may not function for regulating stiffness until this stage, consistent with our findings that FGFR is not phosphorylated at this time (Figures 6A and 6B). Taken together, we propose a model in which mechanical force activates the FGFR-Erk2 pathway and induces junction remodeling, and this mechanochemical system functions in epiboly movement during normal gastrulation, which confers stiffness and integrity of the ectodermal tissue (Figure 7F).

DISCUSSION

In addition to the regulation of gene transcription and translation and the resulting exerted protein functions, it is increasingly important to understand how physical environments influence biological phenomena, as we have learned from previous reports using cultured cells (Engler et al., 2006; Kim et al., 1999; Pelham and Wang, 1997). Furthermore, a growing body of evidence also suggests that physical forces generated in the embryo are indispensable for normal morphogenesis during embryogenesis (Barriga et al., 2018; Keller, 2012; Mammoto et al., 2013; Miller and Davidson, 2013; Wozniak and Chen, 2009). Particularly in embryogenesis, groups of differentiated cells—namely, embryonic tissues—migrate vigorously within an embryo and are relocated from one place to another to form various organs, generating pushing, pulling, or friction forces (Heisenberg and Bellaïche, 2013; Miller and Davidson, 2013; Petridou et al., 2017).

To examine the impact of these physical forces, we previously performed a global phosphoproteome analysis, in which we applied mechanical force by centrifugation to developing *Xenopus laevis* embryos and found that the force induced the phosphorylation of numerous proteins (Hashimoto et al., 2019). Furthermore, we found that subsets of proteins implicated in cytoskeleton dynamics become phosphorylated, and the phosphoproteomic profile suggested that mechanical force induces a transition from a mesenchymal to an epithelial cell state. In the present study, we expanded these findings using *Xenopus* embryos as the experimental system and reported the phenotypes at the cell level.

We first focused on Erk2, which is pivotal in coordinating a variety of extracellular signals, such as growth factors, and confirmed that it became phosphorylated within 10 min of centrifugation, which is considered an early response. Erk2 was previously shown to be activated by fluid shear stress and cyclic mechanical strain in tissue culture cells *in vitro* (Reusch et al., 1997; Tseng et al., 1995). It has been shown that Erk and Rho

Figure 6. FGFR1 and Erk2 Phosphorylation and Junctional Enhancement during Normal Gastrulation

(A) St. 10.5 and 12 embryos and animal caps isolated at st. 9 and cultured until sibling embryos reached at st. 12 were immunostained with anti-pFGFR antibodies. The animal pole region of st. 10 embryos and the anterior region of st. 12 embryos were observed. Scale bar: 50 μm.

(B) St. 10.5 and st. 12 embryos were immunostained with anti-pErk antibodies. Scale bar: 50 μm.

(C) FGFR-KRYF or ΔC were expressed with mRFP. At st. 12, embryos were fixed and immunostained with anti-pFGFR antibodies. The dotted lines indicate boundaries of injected and uninjected cells. Scale bar: 50 μm.

(D) St. 10.5 and 12 embryos and animal caps were stained with fluorescent-labeled phalloidin and wheat germ agglutinin (WGA). Scale bar: 50 μm.

(E) Statistical data of (D).

(F) St. 10.5 and 12 embryos and animal caps were immunostained with an anti-C-cadherin and anti-ZO-1 antibodies. Scale bar: 50 μm.

(G) mRNAs encoding FGFR-KRYF and GFP were coinjected in one blastomere of four-cell embryos. At st. 12, embryos were fixed and immunostained with anti-C-cadherin or ZO-1 antibodies. Scale bar: 50 μm.

(H) The intensities of immunostaining on the plasma membrane were quantified (n = 20) and normalized with average of the control group. *$p < 0.01$.

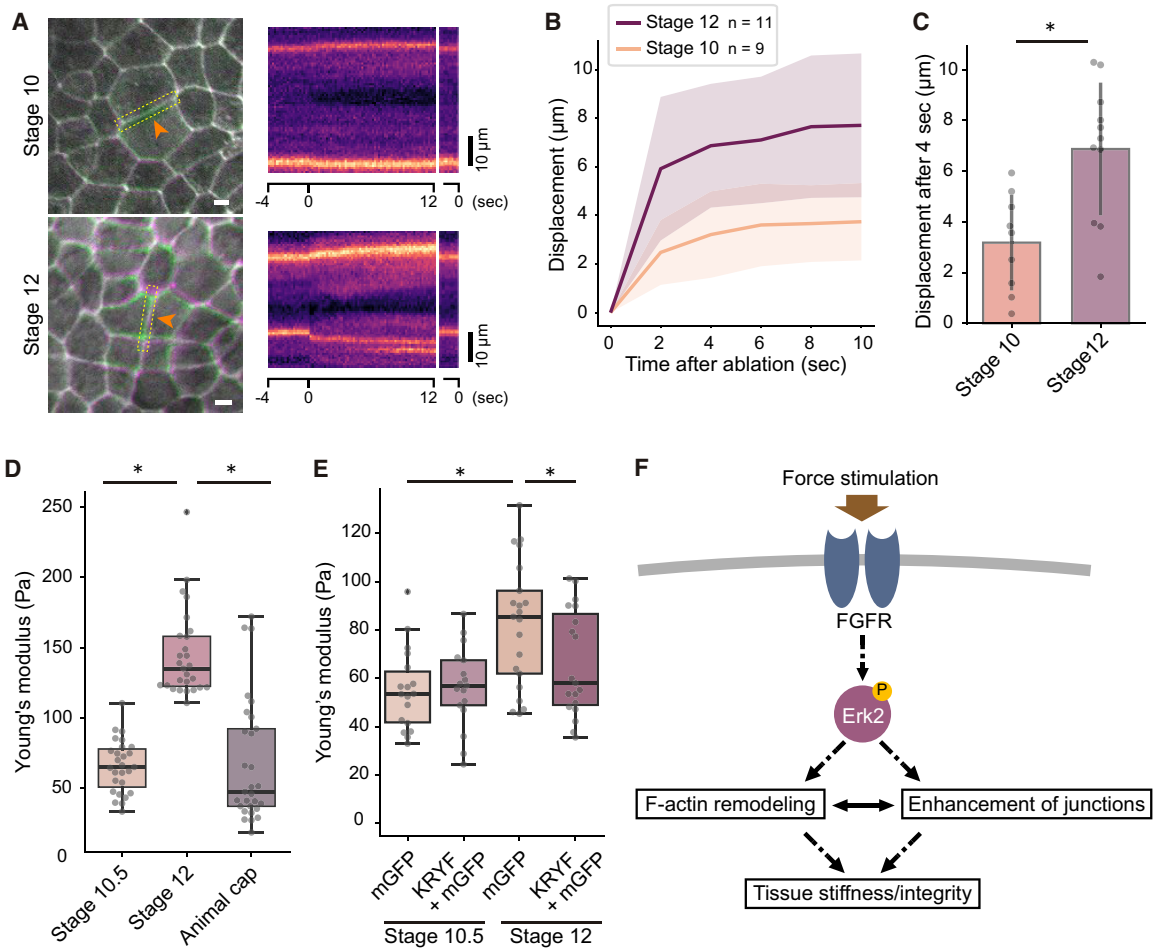

Figure 7. Increase of Cortical Tension and Stiffness during Normal Gastrulation

(A) Laser ablation of the animal pole region of st. 10 embryos and the anterior region of st. 12 embryos. Left panels: images before and 12 s after ablation indicated by green and magenta, respectively, were overlaid. Scale bar: 10 µm. Arrow heads: the ablation points. Right panels: kymographs of the dotted areas in the left panels.

(B) Time-course kinetics of the displacement after laser ablation. n = 9 and 11 for st. 10 and 12 embryos, respectively.

(C) Displacement 4 s after ablation. n = 28 and 34 for st. 10 and 12 embryos, respectively. *p < 0.01.

(D) Stiffness of embryos or animal caps were measured by AFM. St. 10.5 and 12 embryos and animal caps isolated at st. 9 and cultured until sibling embryos reached at st. 12 were used. The animal pole region of st. 10.5 embryos and the anterior region of st. 12 embryos were measured. n = 27 ~29. *p < 0.01.

(E) mGFP alone or FGFR-KRYF and mGFP were expressed at the animal pole region. Stiffness of mGFP-expressing cells were measured at st. 10.5 or 12 by AFM. *p < 0.01.

(F) Graphical summary. Our results demonstrate that the application of mechanical force to ectodermal cells in *Xenopus* embryos activates FGFR in a ligand-independent manner, subsequently activating the Erk2 signaling pathway. This mechanotransduction induces F-actin remodeling and enhancement of cell junctions, which in turn regulate tissue stiffness and integrity.

GTPases are activated and regulate actin cytoskeleton in the wound-healing process in *Xenopus* embryos (Li et al., 2013), raising an interesting question of the difference between the cellular reactions to wound healing and to tissue stretching by mechanical stimuli.

Notably, the centrifugal force induced a remodeling of cytoskeletal components such as F-actin, an embryonic cadherin, C-cadherin, and the tight junction protein ZO-1, which enhanced epithelial cell integrity (Nieto, 2013). In particular, F-actin accumulated at the apical cell surface and enhanced the cortical actin, which we assume was the main cause of the increased cell/tissue stiffness. Because Erk2 is required for F-actin remodeling, and inhibiting Erk2 compromised the centrifugation-induced tissue stiffening, we propose that Erk2 activation initiates a sequence of events from cytoskeletal remodeling to tissue stiffening. It is also reported that ZO-1 changes its conformation in a tension-dependent manner (Spadaro et al., 2017). It is possible that a conformational change of ZO-1 occurs in *Xenopus* embryos and that Erk2 may regulate the process. While it was initially considered that these cellular responses might be induced by the downward movement of subcellular organelles during the centrifugation, we were able to confirm that similar responses were produced by compressing whole embryos or stretching animal cap explants. These findings

indicate that these cellular changes are a common reaction to general physical stresses that cause cellular deformation as a result of tissue expansion.

Finally, an obvious question is how mechanical force triggers Erk2 activation, which leads to the remodeling of cell-cell adhesion and tight junctions. An unexpected finding was that the FGF ligand was dispensable for the force-dependent cellular responses; the force-induced cellular changes were not affected by a dominant-negative FGFR1 that blocks FGF ligands (FGFR-ΔC). This finding was further supported by the observation that isolated animal cap cells, which neither express *FGF4* nor have direct contact with FGF4-producing cells of the mesoderm and endoderm of the marginal zone, showed Erk2 activation upon their centrifugation or stretching. In addition, we found that the FGFR mutant that lacks the FGF-ligand-binding domain (ΔIgΔC110) acts as a dominant-negative inhibitor of FGFR signaling. FGFRs have been reported to be activated independently of ligands when they are mutated or overexpressed (Dieci et al., 2013). Not only the extracellular domain, but also the transmembrane and the cytoplasmic domain, have been implicated in the regulation of the active dimer formation of FGFRs; for example, Grb2 interacting with the cytoplasmic domain of FGFR suppresses ligand-independent FGFR activation (Bocharov et al., 2013; Lin et al., 2012). Our result that the 110-aa cytoplasmic region (ΔC110) of FGFR1 confers the activity of signal inhibition suggests that the cytoplasmic domain may play an important role in the force-induced FGFR activation. Mechanical forces deform the tissue, causing severe changes in the cells' plasma membrane and cytoskeletal networks. Such dynamics may cause conformational changes of FGFRs or other proteins such as ion channels that might functionally associate with FGFRs. In future studies, it will be essential to address in detail how these cellular dynamics activate FGFRs at the molecular level. This research would provide a new avenue for understanding force-dependent signaling pathways (Figure 7F).

Embryogenesis is a dynamic process in which cell-cell interactions and tissue integrity are required for orchestrated cell movements and tissue rearrangements that achieve morphogenesis. Taking our observations in this study altogether, we propose that the remodeling of cytoskeletal proteins in response to physical forces is a cellular reaction that confers in embryonic tissues a resilience to cell and tissue deformation during early development. This resilience is accomplished by enhancing cell junctions and cortical actin, and these changes are critical for the maintenance of tissue integrity in normal development. The tissue integrity, once established by the force, might provide a platform for efficient force transmission, which enables coordinated morphogenesis to occur over an entire tissue. We therefore propose that this mechanical feedback is one of the most important roles of embryonic force.

STAR★METHODS

Detailed methods are provided in the online version of this paper and include the following:

SUPPLEMENTAL INFORMATION

Supplemental Information can be found online at https://doi.org/10.1016/j.celrep.2020.02.074.

ACKNOWLEDGMENTS

This research was supported by KAKENHI 22127007 and 15H05865 from MEXT and JSPS to N.U. and by NIH R01HL135007 to I.M.C. The collaboration among N.U, N.K., Y.H., and I.M.C. is also supported by the NINS Strategic International Research Exchange Promotion Program. The authors deeply thank NIBB Functional Genomics Facility for their technical support in proteomic analyses.

AUTHOR CONTRIBUTIONS

N.K., Y.H., I.M.C., and N.U. designed research. N.K. and Y.H. performed experiments and analyzed data. N.Y. and M.S. performed AFM analyses. N.K., Y.H., I.M.C., and N.U. wrote, edited, and reviewed the manuscript.

DECLARATION OF INTERESTS

The authors declare no competing interests.

Received: March 26, 2019
Revised: January 31, 2020
Accepted: February 19, 2020
Published: March 17, 2020

REFERENCES

Amaya, E., Musci, T.J., and Kirschner, M.W. (1991). Expression of a dominant negative mutant of the FGF receptor disrupts mesoderm formation in Xenopus embryos. Cell *66*, 257–270.

Barone, M.V., and Courtneidge, S.A. (1995). Myc but not Fos rescue of PDGF signalling block caused by kinase-inactive Src. Nature *378*, 509–512.

Barriga, E.H., Franze, K., Charras, G., and Mayor, R. (2018). Tissue stiffening coordinates morphogenesis by triggering collective cell migration in vivo. Nature *554*, 523–527.

Bocharov, E.V., Lesovoy, D.M., Goncharuk, S.A., Goncharuk, M.V., Hristova, K., and Arseniev, A.S. (2013). Structure of FGFR3 transmembrane domain dimer: implications for signaling and human pathologies. Structure *21*, 2087–2093.

Camacho, C., Coulouris, G., Avagyan, V., Ma, N., Papadopoulos, J., Bealer, K., and Madden, T.L. (2009). BLAST+: architecture and applications. BMC Bioinformatics *10*, 421.

Campinho, P., Behrndt, M., Ranft, J., Risler, T., Minc, N., and Heisenberg, C.P. (2013). Tension-oriented cell divisions limit anisotropic tissue tension in epithelial spreading during zebrafish epiboly. Nat. Cell Biol. *15*, 1405–1414.

Chan, C.J., Costanzo, M., Ruiz-Herrero, T., Mönke, G., Petrie, R.J., Bergert, M., Diz-Muñoz, A., Mahadevan, L., and Hiiragi, T. (2019). Hydraulic control of mammalian embryo size and cell fate. Nature *571*, 112–116.

Chen, R.H., Sarnecki, C., and Blenis, J. (1992). Nuclear localization and regulation of erk- and rsk-encoded protein kinases. Mol. Cell. Biol. *12*, 915–927.

Clark, S.G., Stern, M.J., and Horvitz, H.R. (1992). C. elegans cell-signalling gene sem-5 encodes a protein with SH2 and SH3 domains. Nature *356*, 340–344.

Davidson, L.A., Hoffstrom, B.G., Keller, R., and DeSimone, D.W. (2002). Mesendoderm extension and mantle closure in Xenopus laevis gastrulation: combined roles for integrin alpha(5)beta(1), fibronectin, and tissue geometry. Dev. Biol. *242*, 109–129.

Dieci, M.V., Arnedos, M., Andre, F., and Soria, J.C. (2013). Fibroblast growth factor receptor inhibitors as a cancer treatment: from a biologic rationale to medical perspectives. Cancer Discov. *3*, 264–279.

Engler, A.J., Sen, S., Sweeney, H.L., and Discher, D.E. (2006). Matrix elasticity directs stem cell lineage specification. Cell *126*, 677–689.

Farrell, B., and Breeze, A.L. (2018). Structure, activation and dysregulation of fibroblast growth factor receptor kinases: perspectives for clinical targeting. Biochem. Soc. Trans. *46*, 1753–1770.

Furge, K.A., Kiewlich, D., Le, P., Vo, M.N., Faure, M., Howlett, A.R., Lipson, K.E., Vande Woude, G.F., and Webb, C.P. (2001). Suppression of Ras-mediated tumorigenicity and metastasis through inhibition of the Met receptor tyrosine kinase. Proc. Natl. Acad. Sci. USA *98*, 10722–10727.

Guagnano, V., Furet, P., Spanka, C., Bordas, V., Le Douget, M., Stamm, C., Brueggen, J., Jensen, M.R., Schnell, C., Schmid, H., et al. (2011). Discovery of 3-(2,6-dichloro-3,5-dimethoxy-phenyl)-1-{6-[4-(4-ethyl-piperazin-1-yl)-phenylamin o]-pyrimidin-4-yl}-1-methyl-urea (NVP-BGJ398), a potent and selective inhibitor of the fibroblast growth factor receptor family of receptor tyrosine kinase. J. Med. Chem. *54*, 7066–7083.

Gupta, R.W., and Mayer, B.J. (1998). Dominant-negative mutants of the SH2/SH3 adapters Nck and Grb2 inhibit MAP kinase activation and mesoderm-specific gene induction by eFGF in Xenopus. Oncogene *17*, 2155–2165.

Hara, Y., Nagayama, K., Yamamoto, T.S., Matsumoto, T., Suzuki, M., and Ueno, N. (2013). Directional migration of leading-edge mesoderm generates physical forces: Implication in Xenopus notochord formation during gastrulation. Dev. Biol. *382*, 482–495.

Hashimoto, Y., Kinoshita, N., Greco, T.M., Federspiel, J.D., Jean Beltran, P.M., Ueno, N., and Cristea, I.M. (2019). Mechanical Force Induces Phosphorylation-Mediated Signaling that Underlies Tissue Response and Robustness in Xenopus Embryos. Cell Syst. *8*, 226–241.e227.

Heisenberg, C.P., and Bellaïche, Y. (2013). Forces in tissue morphogenesis and patterning. Cell *153*, 948–962.

Hernández-Vega, A., Marsal, M., Pouille, P.A., Tosi, S., Colombelli, J., Luque, T., Navajas, D., Pagonabarraga, I., and Martín-Blanco, E. (2017). Polarized cortical tension drives zebrafish epiboly movements. EMBO J. *36*, 25–41.

Hiramatsu, R., Matsuoka, T., Kimura-Yoshida, C., Han, S.W., Mochida, K., Adachi, T., Takayama, S., and Matsuo, I. (2013). External mechanical cues trigger the establishment of the anterior-posterior axis in early mouse embryos. Dev. Cell *27*, 131–144.

Hornbeck, P.V., Zhang, B., Murray, B., Kornhauser, J.M., Latham, V., and Skrzypek, E. (2015). PhosphoSitePlus, 2014: mutations, PTMs and recalibrations. Nucleic Acids Res. *43*, D512–D520.

Isaacs, H.V., Tannahill, D., and Slack, J.M. (1992). Expression of a novel FGF in the Xenopus embryo. A new candidate inducing factor for mesoderm formation and anteroposterior specification. Development *114*, 711–720.

Keller, R. (2012). Developmental biology. Physical biology returns to morphogenesis. Science *338*, 201–203.

Kim, B.S., Nikolovski, J., Bonadio, J., and Mooney, D.J. (1999). Cyclic mechanical strain regulates the development of engineered smooth muscle tissue. Nat. Biotechnol. *17*, 979–983.

Levitzki, A., and Gazit, A. (1995). Tyrosine kinase inhibition: an approach to drug development. Science *267*, 1782–1788.

Li, J., Zhang, S., Soto, X., Woolner, S., and Amaya, E. (2013). ERK and phosphoinositide 3-kinase temporally coordinate different modes of actin-based motility during embryonic wound healing. J. Cell Sci. *126*, 5005–5017.

Lin, C.C., Melo, F.A., Ghosh, R., Suen, K.M., Stagg, L.J., Kirkpatrick, J., Arold, S.T., Ahmed, Z., and Ladbury, J.E. (2012). Inhibition of basal FGF receptor signaling by dimeric Grb2. Cell *149*, 1514–1524.

Mammoto, T., Mammoto, A., and Ingber, D.E. (2013). Mechanobiology and developmental control. Annu. Rev. Cell Dev. Biol. *29*, 27–61.

Miller, C.J., and Davidson, L.A. (2013). The interplay between cell signalling and mechanics in developmental processes. Nat. Rev. Genet. *14*, 733–744.

Mohammadi, M., Dikic, I., Sorokin, A., Burgess, W.H., Jaye, M., and Schlessinger, J. (1996). Identification of six novel autophosphorylation sites on fibroblast growth factor receptor 1 and elucidation of their importance in receptor activation and signal transduction. Mol. Cell. Biol. *16*, 977–989.

Mohammadi, M., McMahon, G., Sun, L., Tang, C., Hirth, P., Yeh, B.K., Hubbard, S.R., and Schlessinger, J. (1997). Structures of the tyrosine kinase domain of fibroblast growth factor receptor in complex with inhibitors. Science *276*, 955–960.

Nieto, M.A. (2013). Epithelial plasticity: a common theme in embryonic and cancer cells. Science *342*, 1234850.

Nieuwkoop, P.D., and Faber, J. (1975). Normal Table of Xenopus laevis (Daudin) (Garland Publishing).

Pelham, R.J., Jr., and Wang, Y.l. (1997). Cell locomotion and focal adhesions are regulated by substrate flexibility. Proc. Natl. Acad. Sci. USA *94*, 13661–13665.

Peng, H.B. (1991). Xenopus laevis: Practical uses in cell and molecular biology. Solutions and protocols. Methods Cell Biol. *36*, 657–662.

Petridou, N.I., Spiró, Z., and Heisenberg, C.P. (2017). Multiscale force sensing in development. Nat. Cell Biol. *19*, 581–588.

Plotnikov, A.N., Schlessinger, J., Hubbard, S.R., and Mohammadi, M. (1999). Structural basis for FGF receptor dimerization and activation. Cell *98*, 641–650.

Ramos, J.W., Whittaker, C.A., and DeSimone, D.W. (1996). Integrin-dependent adhesive activity is spatially controlled by inductive signals at gastrulation. Development *122*, 2873–2883.

Reusch, H.P., Chan, G., Ives, H.E., and Nemenoff, R.A. (1997). Activation of JNK/SAPK and ERK by mechanical strain in vascular smooth muscle cells depends on extracellular matrix composition. Biochem. Biophys. Res. Commun. *237*, 239–244.

Seger, R., and Krebs, E.G. (1995). The MAPK signaling cascade. FASEB J. *9*, 726–735.

Shook, D.R., Kasprowicz, E.M., Davidson, L.A., and Keller, R. (2018). Large, long range tensile forces drive convergence during *Xenopus* blastopore closure and body axis elongation. eLife *7*, e26944.

Spadaro, D., Le, S., Laroche, T., Mean, I., Jond, L., Yan, J., and Citi, S. (2017). Tension-Dependent Stretching Activates ZO-1 to Control the Junctional Localization of Its Interactors. Curr. Biol *27*, 3783–3795.e3788.

Tseng, H., Peterson, T.E., and Berk, B.C. (1995). Fluid shear stress stimulates mitogen-activated protein kinase in endothelial cells. Circ. Res. *77*, 869–878.

Weber, G.F., Bjerke, M.A., and DeSimone, D.W. (2012). A mechanoresponsive cadherin-keratin complex directs polarized protrusive behavior and collective cell migration. Dev. Cell *22*, 104–115.

Winklbauer, R. (2012). Cadherin function during Xenopus gastrulation. Subcell. Biochem. *60*, 301–320.

Wozniak, M.A., and Chen, C.S. (2009). Mechanotransduction in development: a growing role for contractility. Nat. Rev. Mol. Cell Biol. *10*, 34–43.

Xiong, F., Ma, W., Benazeraf, B., Mahadevan, L., and Pourquie, O. (2018). Mechanical coupling coordinates the co-elongation of axial and paraxial tissues in avian embryos. bioRxiv. https://doi.org/10.1101/412866.

Zhou, J., Pal, S., Maiti, S., and Davidson, L.A. (2015). Force production and mechanical accommodation during convergent extension. Development *142*, 692–701.

STAR★METHODS

KEY RESOURCES TABLE

REAGENT or RESOURCE	SOURCE	IDENTIFIER
Antibodies		
anti-phosphoErk1/2 antibody	Cell Signaling Technology	cat. # 4370; RRID:AB_2315112
anti-phoshoErk antibody	Santa Cruz Biotechnology	cat. # sc-7383; RRID:AB_627545
anti-Erk1/2 antibody	Cell Signaling Technology	cat. # 4695; RRID:AB_390779
anti-phosphoFGFR 1 antibody	Cell Signaling Technology	cat. # 3471; RRID:AB_331072
anti-ZO-1 antibody	Thermo Fisher Scientific	cat. # 33-9100; RRID:AB_2533147
anti-C-cadherin antibody	Development Studies Hybridoma Bank	cat. # 6B6; RRID:AB_528113
goat anti-mouse IgG antibody, Alexa Fluor 488	Thermo Fisher Scientific	cat. # A28175; RRID:AB_2536161
goat anti-mouse IgG antibody, Alexa Fluor 555	Thermo Fisher Scientific	cat. # A28180; RRID:AB_2536164
goat anti-rabbit IgG antibody, Alexa Fluor 488	Thermo Fisher Scientific	cat. # A11008; RRID:AB_143165
goat anti-rabbit IgG antibody, Alexa Fluor 555	Thermo Fisher Scientific	cat. # A27039; RRID:AB_2536100
alkaline phosphatase-conjugated anti-mouse IgG antibody	Thermo Fisher Scientific	cat. # 31321; RRID:AB_10959407
alkaline phosphatase-conjugated anti-rabbit IgG antibody	Thermo Fisher Scientific	cat. # 31340; RRID:AB_228339
Chemicals, Peptides, and Recombinant Proteins		
proteinase K	Wako	cat.# 160-14001
fibronectin	Sigma-Aldrich	cat. # F1141
PD0325901	Sigma-Aldrich	cat. # PZ0162
SU5402	Wako	cat. # 197-16731
BGJ398	ChemScene	cat. # CS-0586
anisomycin	Sigma-Aldrich	cat. # A9789
cycloheximide	Sigma-Aldrich	cat. # C7698
goat serum	MBL Lifescience	cat.# SG30-0500
Alexa Fluor 546 Phalloidin	Thermo Fisher Scientific	cat.# A22283; RRID:AB_2632953
Hoechst 33342	abcam	cat.# ab228551
Critical Commercial Assays		
MESSAGE MACHINE SP6 Transcription Kit	Thermo Fisher Scientific	cat. # AM1340
Deposited Data		
DDA data	Hashimoto et al., 2019	PRIDE: PXD010676
Experimental Models: Organisms/Strains		
Xenopus laevis (J-strain)	N/A	N/A
Recombinant DNA		
Xenopus laevis FGF receptor 1	Amaya et al., 1991	GenBank: U24491.1
FGFRΔC (1-397 aa)	This paper	N/A
FGFR1-KRYF (K508R/Y647F/Y648F)	This paper	N/A
FGFRΔC110 (1-507 aa)	This paper	N/A
FGFRΔIgΔC110 (1-507 aa with deletion of 121-274 aa)	This paper	N/A
Xenopus laevis GRB2	XL274b24ex	http://xenopus.nibb.ac.jp
GRB2-SH2 (58-161 aa)	This paper	N/A
Software and Algorithms		
BLAST+	NIH	ftp://ftp.ncbi.nlm.nih.gov/blast/executables/blast+
Fiji	NIH	https://fiji.sc

(*Continued on next page*)

Continued

REAGENT or RESOURCE	SOURCE	IDENTIFIER
ProteomeDiscoverer 2.2	Thermo Fisher Scientific	https://www.thermofisher.com/order/catalog/product/OPTON-30795
Python 3.6	Python Core Team	https://www.python.org
Pandas	v0.22	https://pandas.pydata.org
seaborn	v0.8	https://seaborn.pydata.org
Matplotlib	v2.2	https://matplotlib.org
SciPy	v1.0	https://www.scipy.org
Andor IQ2	Oxford Instruments	https://andor.oxinst.com/products/iq-live-cell-imaging-software/
JPK data processing	JPK Instruments	https://jpk-data-processing.updatestar.com

LEAD CONTACT AND MATERIALS AVAILABILITY

Further information and requests for resources and reagents should be directed to and will be fulfilled by Lead Contact, Naoto Ueno (nueno@nibb.ac.jp.). All unique/stable reagents generated in this study are available from the Lead Contact with a completed Material Transfer Agreement.

EXPERIMENTAL MODEL AND SUBJECT DETAILS

Xenopus embryos

Xenopus laevis eggs were obtained from females injected with 400 IU of human chorionic gonadotrophin (Takeda Pharm., Japan), and were fertilized *in vitro*. Eggs were dejellied with 3% cysteine hydrochloride (pH 8.0), and embryos were subjected to microinjection in 0.1 × Steinberg's solution (Peng, 1991) containing 3% Ficoll 400. The embryos were staged according to Nieuwkoop and Faber (1975).

Inhibitors and antibodies

PD0325901 (cat. # PZ0162, Sigma) was dissolved in DMSO at 50 mM. SU5402 (cat. # 197-16731, Wako, Japan) and BGJ398 (cat. # CS-0586, ChemScene, NJ, USA) were dissolved in DMSO at 10 mM. Anisomycin (cat. # A9789, Sigma) and cycloheximide (cat. # C7698, Sigma) were dissolved in DMSO at 5 mg/ml.

Primary antibodies used in this study were: anti-pErk1/2 (cat. # 4370, Cell Signaling Technology (CST)), anti-pErk (cat. # sc-7383, Santa Cruz Biotechnology), anti-Erk1/2 (cat. # 4695, CST), anti-pFGFR (cat. # 3471, CST), anti-ZO-1 (cat. # 33-9100, Thermo Fisher Scientific), and anti-C-cadherin (cat. # 6B6, Development Studies Hybridoma Bank).

Secondary antibodies for immunofluorescence were goat anti-mouse antibody Alexa Fluor 488 and 555 (cat. # A28175 and A28180, respectively, Thermo Fisher Scientific) and goat anti-rabbit IgG antibody Alexa Fluor 488 and 555 (cat. # A11008 and A27039, respectively, Thermo Fisher Scientific). For western blotting, alkaline phosphatase-conjugated anti-mouse and anti-rabbit IgG antibodies (cat. # 31321 and 31340, respectively, Thermo) were used.

METHOD DETAILS

Xenopus embryo manipulations

To apply centrifugal force to embryos, the embryos were treated with 10 μg/ml proteinase K (cat.# 160-14001, Wako, Japan) in 0.3 × MMR (Peng, 1991) for 15 to 30 minutes at st. 9, washed three times, and incubated until they reached st. 10.5. For centrifugation of embryos, 35 mm-diameter dishes coated with 1 mL of 0.8% agarose in 0.3 × MMR were used. Embryos in 0.3 × MMR were placed on the agarose gel, and centrifuged at 15°C using Kubota 6200 centrifuge with a PF-206 rotor. Although the centrifugation flattened the embryos drastically, they recovered from the severe morphological changes, and developed to apparently normal embryos (44/53 for centrifugation and 16/21 for compression).For fixation for immunofluorescence, 1/4 volume of 5 × concentrated MEMFA (0.1 M MOPS (pH 7.4), 2 mM EGTA, 1mM magnesium Sulfate and 3.7% formaldehyde) was added.

To apply the compression force, proteinase K-treated embryos were placed between 0.3- or 0.5-mm-thick spacers, and then compressed with a cover glass and 17 g weight for 5 minutes. For fixation for immunofluorescence, the cover glass was removed and 1/4 volume of 5 × concentrated MEMFA was immediately added to the dish. To apply the stretch force, silicone chambers (cat. # STB-CH-0.02, STREX Inc, Osaka, Japan) were coated with fibronectin (cat. # F1141, Sigma). It was coated with 10 μL of 0.2 mg/ml fibronectin solution, excess solution was removed, and then it was dried in air. For the stretch, the chamber was manually stretched to 1.5-fold in length and hold for 5 minutes. For fixation for immunofluorescence, the stretched chamber was released, and 1/4 volume of 5 × concentrated MEMFA was immediately added to the chamber.

This study was carried out in strict accordance with the Guide for the Care and Use of Laboratory Animals of the National Institute for Basic Biology. The protocol was approved by the Institutional Animal Care and Use Committee of the National Institutes of Natural Sciences (Permit Number: 18A015).

Immunofluorescence microscopy

Embryos were fixed in MEMFA (0.1 M MOPS (pH 7.4), 2 mM EGTA, 1mM magnesium Sulfate and 3.7% formaldehyde) for 2 hours at room temperature or overnight at 4°C, and washed 3 times in PBS-0.1% Tween 20 (PBSTw). The embryos were then bleached with 10% hydrogen peroxide in methanol, except in the case of fluorescent phalloidin staining, and washed 3 times in PBS-0.1% Triton X-100. Blocking was done with 20% goat serum (cat # SG30-0500, MBL, Japan) in PBSTw for one hour at room temperature. Primary and secondary antibodies were diluted 200 times in the blocking solution. The embryos were then incubated in the antibody solution at 4°C overnight. After washing 3 times, the embryos were observed. For microscopic observation, the embryos were placed on a glass-bottom dish and observed by a laser-scanning confocal microscope (Leica SP8). Images were analyzed using the Leica SP8 software, ImageJ (https://imagej.nih.gov/ij/), and Fiji (https://fiji.sc).

Plasmid construction and *in vitro* transcription

To construct the Grb2-SH2 expression plasmid, the region encoding the SH2 domain (58-161 aa) was amplified by PCR using the clone XL274b24ex (http://xenopus.nibb.ac.jp), which contains full-length Grb2 cDNA, as a template. The PCR product was ligated into the pCS2+ vector.

cDNA encoding FGFR1 was a gift from Dr. Enrique Amaya (Amaya et al., 1991). The FGFR1 mutants, FGFRΔC (1-397 aa), FGFR1-KRYF which has K508R/Y647F/Y648F mutations, FGFRΔC110 (1-507 aa) and FGFRΔIgΔC110 (1-507 aa with deletion of the 121-274 aa region), were constructed by PCR-based mutagenesis. For *in vitro* transcription, the MESSAGE MACHINE SP6 Transcription Kit (cat. # AM1340, Thermo Fisher Scientific) was used.

QUANTIFICATION AND STATISTICAL ANALYSIS

Data analysis of Erk2 substrates from proteomics data

Phosphoproteome data were derived from PRIDE: PXD010676 of the PRIDE partner repository. Phosphosites of Erk2 substrates were obtained from PhosphoSitePlus (Hornbeck et al., 2015) as peptide sequences of 15 amino acids in length (downloaded in February 2017) and were searched for homology with *Xenopus laevis* protein sequences in the *Xenopus laevis* protein background (v9.1, gene model: 1.8.3.2) using BLAST+ (Camacho et al., 2009). Each phosphosite was normalized to the individual protein abundance. The distribution of the normalized phosphosite ratio under the force-stimulated condition to that under the normal condition was fitted to a normal distribution using the SciPy and Matplotlib python packages. A heatmap plot was constructed using seaborn python packages.

Atomic force microscopy (AFM) measurements

AFM measurements were conducted with a JPK Nanowizard Cellhesion 200 (JPK Instruments AG, Germany) fitted to Axio Zoom V. 16 system (Zeiss). Cantilevers were customized; silicon nitride AFM probes, 0.02 N/m cantilever with 10 μm SiO_2 particle (Novascan, USA). Young's modulus was calculated using JPK data processing software (JPK Instruments). The measurement condition was as follows; set point 1.5-5.0 nN, approach speed 2 or 5 μm/s, data rate 500 or 1000 Hz, measured spring constant 0.016-0.018 N/m. *Xenopus* embryos were treated with 10 μg/ml of proteinase K for 15 minutes at st. 9, and then the vitelline membrane was manually removed. Embryos were placed in 0.3 × MMR on a plastic dish coated with 1% agarose and 3-9 points per embryo were measured.

Laser ablation

100 pg of mRNA encoding mGFP was injected near the animal pole of two blastomeres of 2-cell embryos. The vitelline membrane was manually removed at st. 9 and cultured until indicated stages. Laser ablation was conducted as described previously (Hara et al., 2013), using an Olympus IX 81 inverted microscope (20 × /0.70 NA dry objective lens), equipped with a spinning-disc confocal unit Yokogawa CSUX-1 and iXon3 897 EM-CCD camera (Andor), controlled with Andor IQ2 software. An N2 Micropoint laser (16 Hz, 365 nm, Photonic Instruments) was focused on membrane at a cell-cell contact site labeled with mGFP. Time lapse images were acquired every 200 msec before and during the course of the laser ablation process and analyzed with Fiji software. Kymographs were generated using Rescilce command from Fiji and slice count set as 10. Heatmap of resulting kymographs were based on fluorescence intensity and generated with "magma" colormap of Matplotlib python package.

DATA AND CODE AVAILABILITY

Proteomics data have been deposited to the ProteomeXchange Consortium via the PRIDE partner repository with the dataset identifier PRIDE: PXD010676 (Hashimoto et al., 2019). Any additional data is available upon request.